Thermoconvective instabilities of a non-uniform Joule-heated high Prandtl number liquid

F. Pigeonneau

MINES ParisTech - CEMEF - Centre for Material Forming, CS 10207, Rue Claude Daunesse 06904 Sophia Antipolis Cedex, France

Résumé :

Cette étude numérique porte la convection naturelle produite lorsqu'un liquide est chauffé par effet Joule. Le modèle est basé sur le couplage entre les équations de Navier-Stokes écrites dans le cadre de l'approximation de Boussinesq, l'équation de conservation de l'énergie et celle du potentiel électrique. Le problème est résolu numériquement à l'aide d'une méthode élément fini en formulation standard et Galerkin discontinu. Deux paramètres contrôlent les phénomènes de transfert : le premier est le nombre de Rayleigh Ra *basé sur une échelle de température prenant en compte la puissance dissipée et le deuxième est le nombre de Prandtl* Pr *considéré toujours supérieur ou égal à un. Le domaine de calcul est une cavité rectangulaire bidimensionnelle dont la longueur est prise deux fois plus grande que la hauteur. Le champ électrique est produit grâce à l'application d'un potentiel sur deux électrodes correspondant à une fraction des parois verticales de la cavité. La paroi horizontale supérieure est soumise à une température uniforme.*

Quand les électrodes ont une longueur égale à la hauteur de la cavité, la convection se produit au delà d'une valeur seuil de Ra *indépendante du nombre de Prandtl. La nature de l'instabilité est analysée en étudiant l'intensité de l'écoulement mesurée en terme de nombre de Péclet.*

Une étude de la convection est faite lorsque les électrodes ont une longueur égale à $2/3$ *de la hauteur. Dans ce cas, la convection apparaît sans seuil. Deux régimes d'écoulement émergent : un régime « conductif » valide quand* $\mathrm{Ra} < 10^3$ *pour lequel le nombre de Péclet est proportionnel à* Ra *et un régime « convectif » pour lequel le nombre de Péclet est une fonction de la racine carrée du nombre de Rayleigh. Une instabilité thermoconvective apparaît au cours de laquelle l'écoulement qui à faible* Ra *présente une structure symétrique devient asymétrique au delà d'une certaine valeur du nombre de Rayleigh. La valeur critique de* Ra *de cette transition dépend fortement de* Pr *pour les faibles valeurs du nombre de Prandtl alors qu'elle reste pratiquement constante à grand nombre de Prandtl. L'analyse de l'écoulement pour des valeurs de Rayleigh plus grandes que les valeurs critiques montre que l'écoulement devient périodique en temps et que cette instabilité est semblable à une bifurcation de Hopf.*

Abstract:

This numerical study is devoted to the thermoconvection occurring when a liquid is heated by the Joule dissipation. The model is based on the coupling between the Navier-Stokes equations written in the framework of the Boussinesq approximation, energy equation and electric potential conservation. A numerical solver has been developed using standard and discontinuous Galerkin finite element method. The problem is controlled by the Rayleigh number Ra *in which the temperature scale depends on the*

volumetric source term and by the Prandtl number Pr *which is considered larger than one. The domain is a 2d rectangular cavity with a length equal to twice of the height. The electric field is provided with two vertical electrodes corresponding to a fraction of the vertical walls of the enclosure. A uniform temperature is applied in the upper horizontal wall.*

When the electrode length is equal to the height of the cavity, the convection appears above a critical Rayleigh number independent on the Prandtl number. The nature of the instability is analyzed by studying the motion intensity determined in term of a Péclet number close to the critical Rayleigh number.

We perform a numerical study when the electrode lengths are equal to the $2/3$ *of the cavity height. In this case, the motion appears without threshold. Two regimes of motion are established: the "conductive" regime observed when* $\mathrm{Ra} < 10^3$ *for which the Péclet number is proportional to the Rayleigh number and the "convective" regime in which the Péclet number scales as the square root of* Ra *whatever the Prandtl number. A thermoconvection instability is established in which the symmetric structure of flow breaks down to evolve toward an asymmetric structure. The critical Rayleigh number corresponding to the onset of this transition depends strongly on the Prandtl number when* Pr *is lesser than 3 while for larger values of* Pr*, the critical Rayleigh number becomes independent on* Pr*. By analyzing the flow obtained for Rayleigh numbers larger than the critical values, we pinpoint that the flow becomes periodic in time and the onset of periodic solution obeys to a Hopf bifurcation.*

Mots clefs : thermoconvection, instabilité, effet Joule, méthode élément fini, formulation Galerkin discontinu, four électrique.

1 Introduction

The heating by Joule dissipation is currently employed in various industrial processes such as in glass industry. Electric melting is commonly used for production of potentially volatile, polluting glasses, high added-value products and also in other sectors like wool insulation [16]. One advantage of this process is its high thermal efficiency due to the bulk heat source and its high level of insulation [20]. Due to the molten glass dilatation, free convection appears contributing to the chemical and thermal homogenization of the liquid. The level of the convection depends on the glass properties and is one of the main issues for engineers involved in the furnace design.

Molten glass can be modeled as a Newtonian liquid characterized by a high viscosity. When the temperature is around $1400°C$, the dynamic viscosity is approximately ten thousand times greater than the water viscosity [19]. Moreover, the thermal conductivity is small even if radiation is the main mode of heat transfer [25]. Consequently, one of the main characteristics of the molten glass is the high Prandtl numbers which can be ranged between 10^2 for clear glass up to 10^5 for dark glass. As it was pointed out by Gopalakrishnan et al. [8], the thermal instabilities can appear even if steady conditions are applied in Joule heated cavities. Nevertheless, nothing has been done in the previous contribution to be sure that the instabilities come from the physics and not from the poor numerical resolution.

In order to characterize the nature of the instabilities, it is required to have an accurate solver. Consequently, we develop our own solver to study the thermoconvection instabilities with a volumetric source term. Indeed, from the industrial point of view, it is very important to know parameters leading to unsteady behaviors which can be the source of bad working conditions. In the same spirit of previous
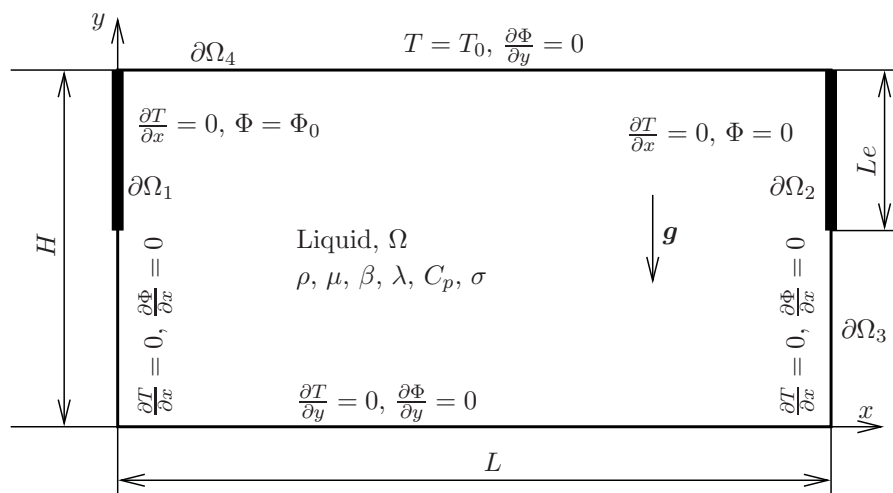
Figure 1: Computational domain Ω, filled with an electric liquid conductor. An electric potential is applied on vertical electrodes, $\partial\Omega_1$ and $\partial\Omega_2$ while a temperature is applied on the top horizontal boundary, $\partial\Omega_4$.

works achieved to study the heat and mass transfer of liquid non-uniformly heated from above in rectangular enclosure [7, 14, 24], we consider a simple cavity heated by Joule effect. The two electrodes are a fraction of the vertical walls of the enclosure.

Section 2 is devoted to the problem statement. The two next sections present results obtained with two configurations: the first corresponds to the case where the electrode length is equal to the cavity height, § 3 and the second when the electrodes length is equal to 2/3 of the height, § 4. Finally, few conclusions will be drawn in section 5.

2   Problem statement

We consider a rectangular cavity of length L and height H filled with an electric conductor liquid. The enclosure is reported to a Cartesian framework (x, y) with unit vectors $\boldsymbol{e}_x$ and $\boldsymbol{e}_y$ along x and y axis respectively. The liquid undergoes a gravity field $\boldsymbol{g} = -g\boldsymbol{e}_y$ as shown in Figure 1. An electric field is provided in the cavity from electrodes corresponding to a fraction of the left and right vertical walls. As depicted in Figure 1, the length of the electrodes is equal to Le. The boundaries $\partial\Omega_1$ and $\partial\Omega_2$ correspond to the left and right electrodes respectively. The electric potential is set equal to $\Phi = \Phi_0$ on the left electrode and $\Phi = 0$ on the right electrode. The boundary $\partial\Omega_3$ is constituted by the rest of the vertical walls and by the bottom horizontal wall taken as an electric and thermal insulator. A uniform temperature T_0 is applied on the top of the enclosure $\partial\Omega_4$. This boundary is also assumed to be an electric insulator. A non-slip boundary condition is applied on the whole frontiers.

The physical properties introduced below are assumed constant. In practice, the electric field is provided by using an alternative current to avoid the fouling of the electrodes. Nevertheless, as pointed out by Stanek [20] and by Choudhary [3], the determination of the electric field is strongly simplified since the unsteadiness of the Maxwell equations can be neglected because the ratio of the typical length of the enclosure is very small compared to the wavelength of the current oscillation. Moreover the magnetic Reynolds number is also very small since the relative magnetic permeability of molten glass is around one. Consequently, the induced magnetic field can be neglected as well meaning that the induced Lorentz

force is also not taking into account according to Gopalakrishna et al. [8]. Under such conditions, the determination of the electric field in the liquid pool can be decoupled of the heat and mass transfer.

Electro-thermo-mechanical properties required in such a problem are the electric conductivity σ, the density ρ defined at the temperature T_0, the dynamic viscosity η, the thermal expansion β, the thermal conductivity λ and the heat capacity C_p. The governing equations of motion are the Navier-Stokes equations with the gravitational body force due to the non-uniform temperature field coupled with the energy balance. Buoyancy force is usually described in the framework of the Boussinesq approximation [2].

Before to introduce the governing equations, a normalization is operated. First the space coordinates are normalized by the height of the enclosure. The electric potential is normalized obviously by Φ_0 and the electric current by $\sigma \Phi_0 / H$. Due to the thermal source term, the temperature T is reduced as follows (see for more detail [13])

$$\theta = \frac{T - T_0}{\Delta T}, \tag{1}$$

with ΔT equal to

$$\Delta T = \frac{\sigma \Phi_0^2 H^2}{2 \lambda L^2}. \tag{2}$$

The scaling of the velocity is determined by considering the balance between the inertial and buoyancy forces leading to the order of the magnitude of the velocity equal to $\sqrt{\beta \Delta T g H}$. Finally, since we consider a situation where the thermal diffusivity $\kappa = \lambda / (\rho C_p)$ is much smaller than the kinematic viscosity $\nu = \eta / \rho$, the time scale is taken equal to H^2 / κ.

With this normalization, the dimensionless governing equations are the following

$$\boldsymbol{\nabla} \cdot \boldsymbol{u} = 0, \tag{3}$$

$$\frac{1}{\mathrm{Pr}} \frac{\partial \boldsymbol{u}}{\partial t} + \sqrt{\frac{\mathrm{Ra}}{\mathrm{Pr}}} \boldsymbol{u} \cdot \boldsymbol{\nabla} \boldsymbol{u} = -\boldsymbol{\nabla} p + \boldsymbol{\nabla}^2 \boldsymbol{u} + \sqrt{\frac{\mathrm{Ra}}{\mathrm{Pr}}} \theta \boldsymbol{e}_y, \tag{4}$$

$$\frac{\partial \theta}{\partial t} + \sqrt{\mathrm{Pr}\,\mathrm{Ra}} \boldsymbol{\nabla} \theta \cdot \boldsymbol{u} = \boldsymbol{\nabla}^2 \theta + 2L^2 \left(\boldsymbol{\nabla} \Phi \right)^2, \tag{5}$$

$$\boldsymbol{\nabla}^2 \Phi = 0, \tag{6}$$

in which $\boldsymbol{u} = (u, v)$ is the dimensionless velocity with u and v the two components along the x and y coordinates respectively. The pressure p takes into account the hydrostatic contribution. Equations (3), (4) and (5) arise from the mass, momentum and energy balances. The Laplace equation (6) comes from the free divergence of the electric current given by the Ohm's law

$$\boldsymbol{J} = -\boldsymbol{\nabla} \Phi, \tag{7}$$

in dimensionless form which gives equation (6) by taking the divergence of the electric current.

In the energy equation (5), the viscous dissipation source term has been neglected. Remind that the last term of the right-hand side of (5) represents the heat source term due to Joule dissipation with L the dimensionless length of the cavity.

Boundary	θ	Φ
$\partial\Omega_1$	$\frac{\partial\theta}{\partial n} = 0$	$\Phi = 1$
$\partial\Omega_2$	$\frac{\partial\theta}{\partial n} = 0$	$\Phi = 0$
$\partial\Omega_3$	$\frac{\partial\theta}{\partial n} = 0$	$\frac{\partial\Phi}{\partial n} = 0$
$\partial\Omega_4$	$\theta = 0$	$\frac{\partial\Phi}{\partial n} = 0$

Table 1: Boundary conditions for θ and Φ on the four frontiers of the enclosure represented in Figure 1.

The dimensionless groups Ra and Pr are respectively the Rayleigh and Prandtl numbers defined by

$$\mathrm{Ra} = \frac{g\beta\Delta T H^3}{\nu\kappa}, \tag{8}$$

$$\mathrm{Pr} = \frac{\nu}{\kappa}. \tag{9}$$

The boundary conditions for θ and Φ are summarized in Table 1 on the four boundaries indicated in Figure 1. For the velocity, only no-slip condition is used on the whole boundaries. Initially, temperature is taken equal to zero in the enclosure and the fluid is assumed to be at rest:

$$\left.\begin{array}{l} \theta(\boldsymbol{x}, 0) = 0, \\ (\boldsymbol{u}, p) = (\boldsymbol{0}, 0), \end{array}\right\} \text{ when } t = 0 \text{ and } \forall \boldsymbol{x} \in \Omega. \tag{10}$$

Equations (3-6) are solved numerally using our own solver developed with the library C++ Rheolef [17]. To solve the Laplace equation (6) which is a pure elliptic equation, a standard Galerkin finite element method has been used for which a polynomial degree is equal to 2 ($\mathbb{P}_2$).

To deal with transport equations, the discontinuous Galerkin finite element method is very well adapted. Indeed, if no numerical smoothing (such as streamline-diffusion or least-squares stabilization) [6] is present in the discretization of the equation, computational modeling with continuous finite elements may lead to poor approximations. In contrast with this behavior, due to their built-in numerical dissipation, no such added numerical diffusion is needed with a discontinuous Galerkin finite element method [5]. Since the Rayleigh number can be larger than one, the advection term in the thermal equation and the non-linear term in Navier-Stokes equations can have a large contribution this is why we choose to employ a discontinuous Galerkin finite element method to solve the Navier-Stokes and the thermal equations. The same polynomial degree equal to 2 ($\mathbb{P}_{2d}$) has been used for $\boldsymbol{u}$, p and θ with an adequate stabilization method to solve the Navier-Stokes equations necessary when the same polynomial degree is used for velocity and pressure [4].

The unsteadiness is considered by taking time derivatives determined with a Backward Differential Formula at the second order (BDF-2) which is unconditionally stable [22]. Since the potential field does not depend on the flow solution, it is solved once and for all before the time integration of the other equations. The coupled equations (3-5) are solved sequentially starting by the thermal equation for which the velocity field is extrapolated at the second order using the forward difference formula [1, Chap. 25]. The non-linear Navier-Stokes problem is numerically solved using a damped Newton method, see for more detail [18]. The numerical computations are driven either when the steady-state is reached or when the time integration is larger than a prescribed time. The steady-state regime is controlled by computing the L^2-norms of the time derivatives of the thermal and velocity fields. We consider that the steady-state regime is reached when the maximum of the L^2-norms is smaller than 10^{-10}. To see more details about

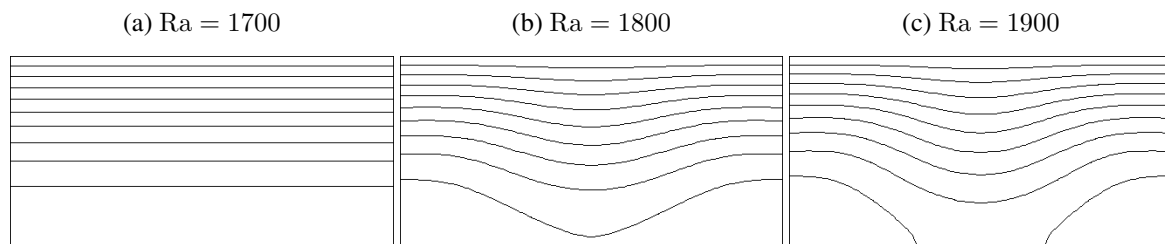(a) Ra = 1700   (b) Ra = 1800   (c) Ra = 1900

Figure 2: Isolines of temperature field in the enclosure for $Le = 1$ and $L = 2$ for $Pr = 1$ with a mesh size $h = 5 \cdot 10^{-2}$ at (a) Ra = 1700, (b) Ra = 1800 and (b) Ra = 1900.
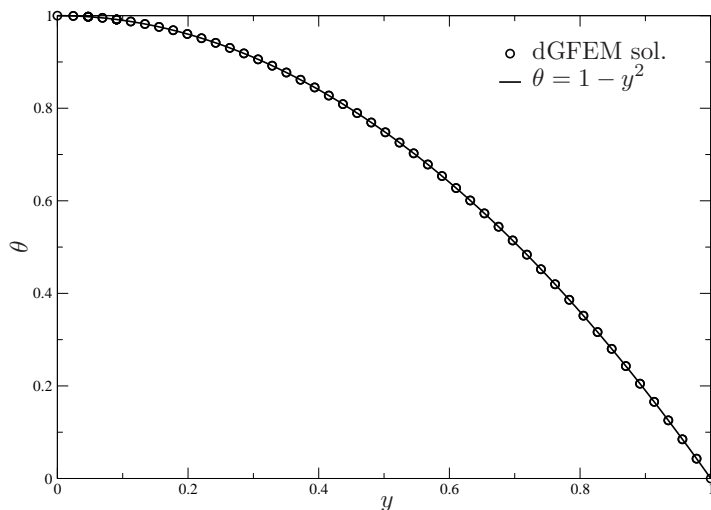

Figure 3: θ as a function of y in the middle of the cavity when Ra = 1700 and $Pr = 1$ for an aspect ratio equal to 2 and $Le = 1$.

the numerical method developed for the present work, report to the reference [13].

3   Numerical results with $Le = 1$

Numerical simulations have been done in a rectangular cavity with a length equal to twice its height and when the electrodes are extended over the whole vertical walls. In such a situation, the electric field is obviously a linear function of x meaning that the Joule dissipation is uniform over the whole enclosure. We performed numerical simulations for three Prandtl numbers equal to 1, 10 and 100.

Figure 2 depicts the temperature field obtained at three values of Rayleigh number when $Pr = 1$. At Ra = 1700, the fluid is at rest since the temperature field does not change over the longitudinal coordinate of the enclosure. Indeed, for a uniform source term without motion, the temperature field depends only on y coordinate as follows

$$\theta = 1 - y^2. \tag{11}$$

Figure 3 depicts the behavior of θ over the y coordinate in the middle of the cavity when the Rayleigh number is equal to 1700 and the Prandtl number is equal to 1. The numerical result provided with circle symbols is compared to the solution (11) in solid line in Figure 3 showing the very good agreement. When the Rayleigh number is equal to 1800 or 1900, temperature isolines are deformed due to the fluid motion.
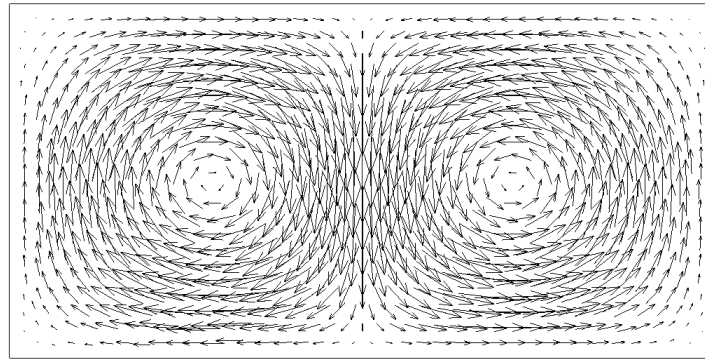
Figure 4: Velocity field in the enclosure for $Le = 1$ and $L = 2$ for $\mathrm{Pr} = 1$ with a mesh size $h = 5 \cdot 10^{-2}$ at $\mathrm{Ra} = 1900$.

Above the critical Rayleigh number, the temperature field is also advected by the fluid in motion. In our solution, the velocity field is structured in two cells with a clockwise rotation for the left cell and an anticlockwise rotation for the right cell as shown in Figure 4.

In order to study more quantitatively the onset of motion, the maximum of the velocity norm found in the cavity is recorded at every time. Due to the normalization used to solve the problem, the velocity must be multiplied by $\sqrt{\mathrm{Ra}\,\mathrm{Pr}}$ to be similar to a Péclet number. In Figure 5, the Péclet number obtained after time convergence is plotted as a function of the Rayleigh number. The velocity in the cavity becomes non-null above a critical Rayleigh number $\mathrm{Ra_{cr}}$. Above $\mathrm{Ra_{cr}}$, $\mathrm{Pe_\infty}$ behaves as a square root of $\mathrm{Ra} - \mathrm{Ra_{cr}}$ as it is also expected in a supercritical bifurcation [12]. By fitting the behavior of the Péclet number as a function of square root of $\mathrm{Ra} - \mathrm{Ra_{cr}}$, the critical Rayleigh number has been found equal to 1701.91. This value is larger than the solution given by Kulacki and Goldstein [11] using a linear stability who found $\mathrm{Ra_{cr}} = 1386$. Nevertheless, the linear stability is achieved in a periodic domain without vertical walls. The finite domain and due to the non-slip boundary condition on every wall strain the fluid to be at rest. Consequently, it is natural to find a larger threshold.

It is noteworthy that the onset of convection is not modified when the Prandtl number changes [10]. Moreover, the amplitude of convection measured in term of $\mathrm{Pe_\infty}$ is the same whatever the Prandtl number demonstrating that the relevant parameter to characterize the motion in the cavity is the Péclet number. This fact is similar to the previous results obtained on horizontal convection [14] and will be justified later.

In the current situation, due to the presence of the source term and the energy conservation, the thermal gradient on the top boundary is imposed and can not be used to define a Nusselt number. According to Roberts [15] and Thirlby [23], the average temperature over the cavity length is introduced as follows

$$\langle\theta\rangle(y,t) = \frac{1}{L}\int_0^L \theta(x,y,t)dx. \tag{12}$$

The Nusselt number is seen as the ratio of the average temperature at the bottom wall without convection to the average temperature at the same location with convection. Since for a uniform volume source term, temperature at the bottom wall is equal to one, the Nusselt number is defined by

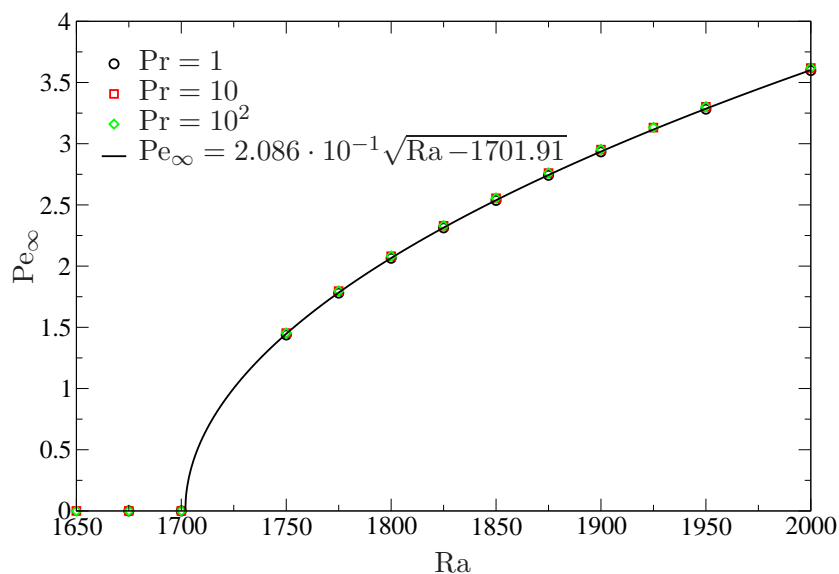$$\mathrm{Nu} = \frac{1}{\langle\theta\rangle(0,t)}. \tag{13}$$

Figure 5: Pe_∞ as a function of Ra for an enclosure of aspect ratio equal to 2 and $Le = 1$ for $Pr = 1$, 10 and 100 obtained numerically on mesh size equal to $h = 5 \cdot 10^{-2}$.

Figure 6 represents the behavior of the Nusselt number around the critical Rayleigh number. Below Ra_{cr}, the Nusselt number is obviously equal to one. Above Ra_{cr}, Nu behaves linearly with $(Ra - Ra_{cr})/Ra_{cr}$. The prefactor obtained by linear regression is close to the prefactor given in [15] equal to 0.599 while our value is equal to 0.544. Remark that Roberts defined the Nusselt number as the average temperature while as Thirlby [23], we choose to use the inverse as given by eq. (13) which leads to an increase of the Nusselt number when the convection is more and more intense.

4   Numerical results with $Le = 2/3$

After these preliminary computations to control the numerical accuracy of our own solver, we performed a numerical study for shorter electrodes with a length taken equal to two third of the vertical size of the enclosure. As in the previous section, numerical simulations are driven until the time convergence.

In a case of short electrodes, the electric current density is not uniform in the cavity leading to a temperature field with a gradient not colinear with the y-axis. Consequently, the motion is expected to appear without threshold. Indeed, according to the criterion proposed by Joseph [9, § 59] telling that the motionless solution exists only if the thermal gradient and the gravity are parallel vector fields. Clearly, this criterion is not fulfilled when $Le < 1$.

Figures 7, 8, and 9 provide the temperature and the stream function respectively for $Ra = 10^2$, 10^4, and 10^5 and for $Pr = 1$. It is noteworthy that the fluid ascends close to electrodes to fall down in the middle of the cavity. Arrows have been reported in sub-figures 7b, 8b, and 9b in order to indicate the sense of the rotation of each cell.

While the temperature field at $Ra = 10^2$ is close to the conductive solution, the advection becomes stronger and stronger at $Ra = 10^4$ and 10^5 to have a main contribution in the solution of the temperature field. When the Rayleigh number is equal to 10^2 and 10^4, the centers of the two vortexes are localized on the horizontal median of the enclosure. For $Ra = 10^5$, the vortex centers go down and are more and more close. In this situation, the flow structure is composed by two counter-rotating cells with a formation of a jet directed downward.
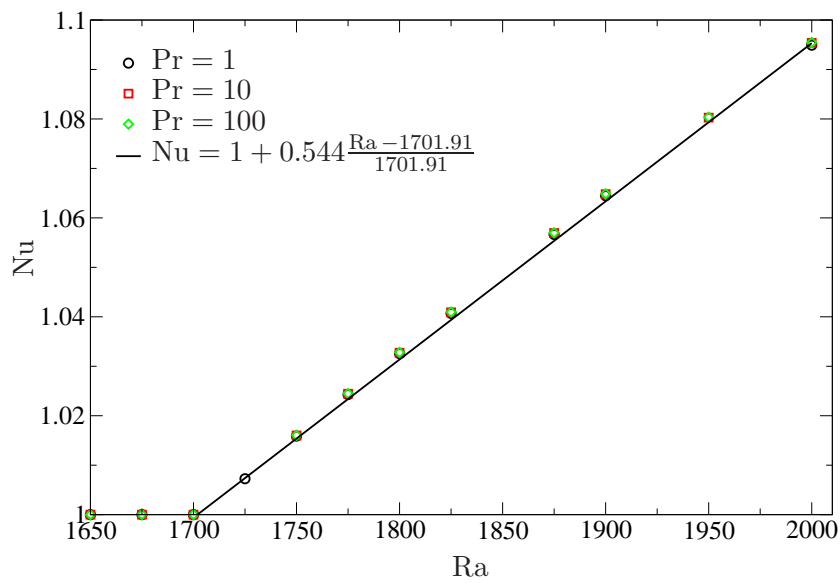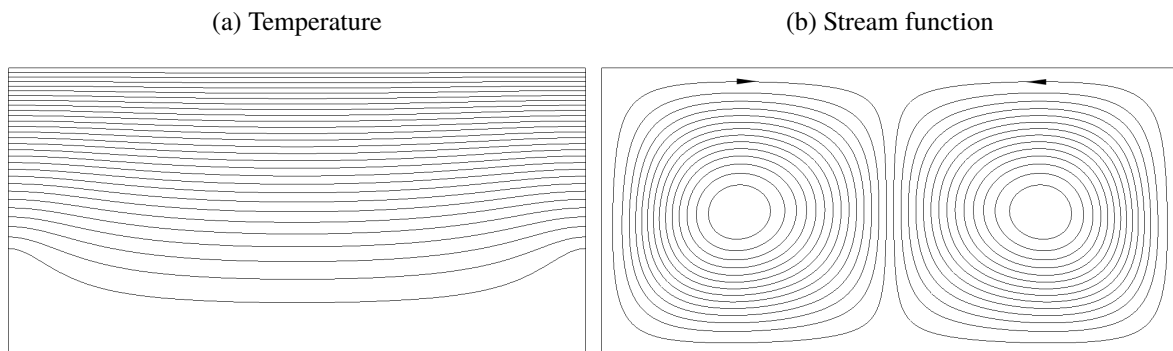
Figure 6: Nu as a function of Ra for an enclosure of aspect ratio equal to 2 and $Le = 1$ for $\mathrm{Pr} = 1, 10$ and 100 obtained numerically on mesh size equal to $h = 2.5 \cdot 10^{-2}$.

(a) Temperature   (b) Stream function

Figure 7: Temperature and stream function obtained after time convergence for $\mathrm{Pr} = 1$, $\mathrm{Ra} = 10^2$ and $Le = 2/3$.

(a) Temperature   (b) Stream function
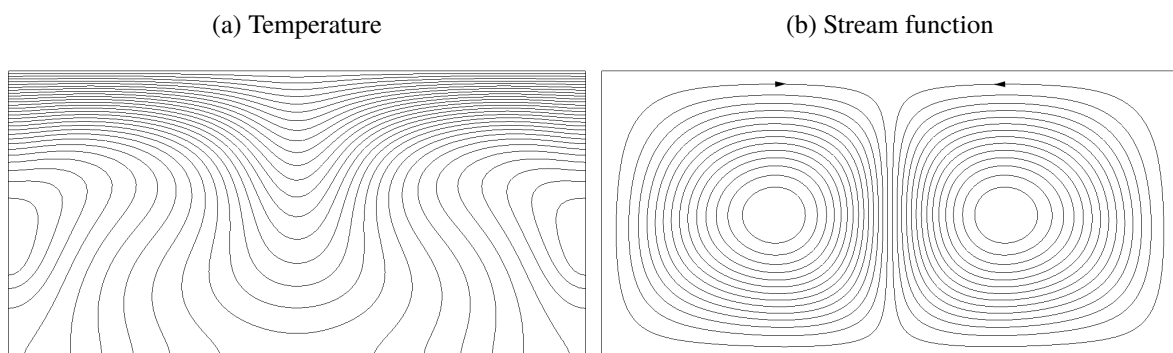
Figure 8: Temperature and stream function obtained after time convergence for $\mathrm{Pr} = 1$, $\mathrm{Ra} = 10^4$ and $Le = 2/3$.

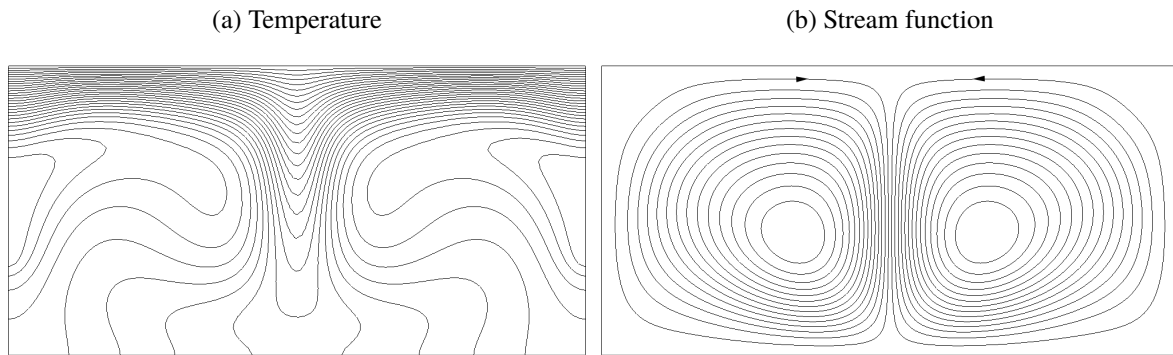(a) Temperature   (b) Stream function

Figure 9: Temperature and stream function obtained after time convergence for $Pr = 1$, $Ra = 10^5$ and $Le = 2/3$.
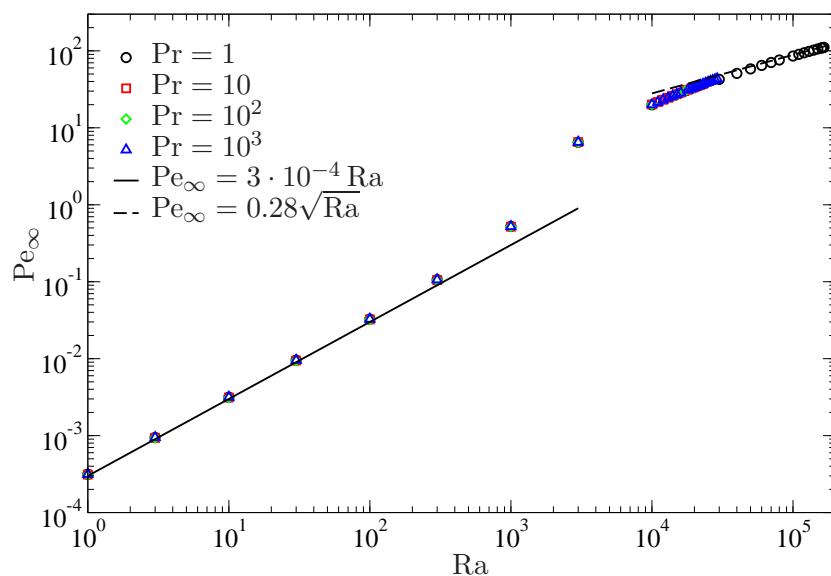

Figure 10: Pe_∞ as a function of Ra for an enclosure of aspect ratio equal to 2 and $Le = 2/3$ for $Pr = 1$, 10, 10^2 and 10^3 obtained numerically on mesh size equal to $h = 2.5 \cdot 10^{-2}$.

This observation of the flow structure indicates that at least two regimes are present in this problem. At low Rayleigh number, the regime is driven by the heat conduction while when the Rayleigh number is large, the temperature field is driven by convection. Figure 10 represents the steady-state Péclet number as a function of the Rayleigh number obtained for four Prandtl numbers. The two regimes are clearly established in Figure 10. When the Rayleigh number is smaller than 10^3, the Péclet number behaves linearly as a function of Rayleigh number. The pre-factor of the curve depends on the length of the electrodes. Above $Ra = 10^3$, a behavior of Pe_∞ changes towards an inertial regime for which the Péclet number scales as a square root of the Rayleigh number.

These two regimes can be explained from a scaling analysis. Indeed, when the Rayleigh number is small, the convection does not play a significant role. Consequently, the viscous term balances the buoyancy term in the momentum equation meaning that the dimensionless velocity scales as $\sqrt{Ra / Pr}$. Since the dimensionless velocity can be seen as the ratio of a Reynolds number to $\sqrt{Ra / Pr}$, it is obvious to observe that the Péclet number scales as the Rayleigh number in the conductive regime.

The second regime is more difficult to explain. Indeed, if we look only the momentum equation, the balance of the inertia and the buoyancy forces gives that the dimensionless velocity is constant mean-
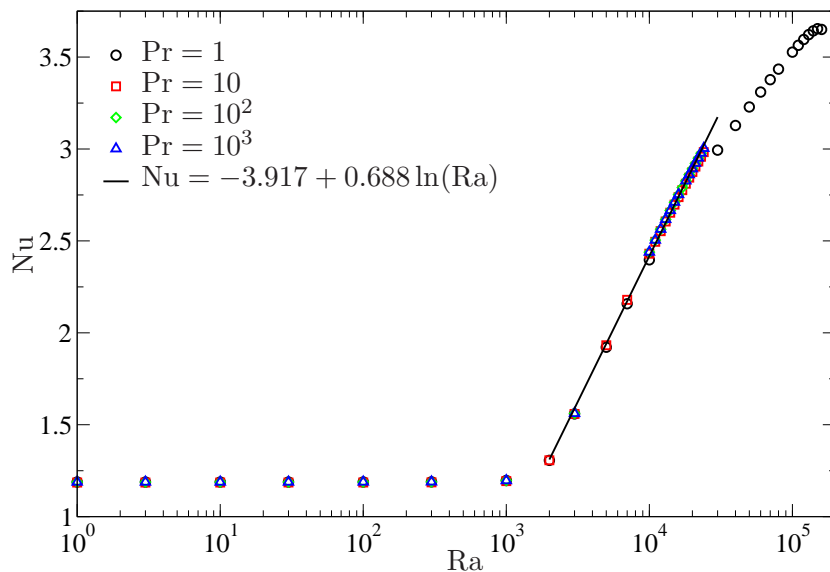
Figure 11: Nu as a function of Ra for an enclosure of aspect ratio equal to 2 and $Le = 2/3$ for $\mathrm{Pr} = 1$, 10, 10^2 and 10^3 obtained numerically on mesh size equal to $h = 2.5 \cdot 10^{-2}$.

ing that with the chosen normalization, the Reynolds number should be proportional to $\sqrt{\mathrm{Ra}\,/\,\mathrm{Pr}}$ and consequently the Péclet number should scale as $\sqrt{\mathrm{Ra}\,\mathrm{Pr}}$ which is not the case. In order to establish the good scaling, it is crucial to take into account the fact that the Prandtl number is larger than one. In this case, the inertia does not play a significant role in the momentum equation meaning that the balance is once again achieved between the viscous and the buoyancy terms as follows

$$u_0 \sim \sqrt{\frac{\mathrm{Ra}}{\mathrm{Pr}}}\,\theta_0, \tag{14}$$

in which u_0 is the order of magnitude of the dimensionless velocity and θ_0 the typical value of the reduced temperature. From the energy equation, the balance at large Rayleigh and Prandtl numbers is given by the convective term and the Joule dissipation such as

$$u_0 \theta_0 \sim \frac{S}{\sqrt{\mathrm{Ra}\,\mathrm{Pr}}}, \tag{15}$$

with S an arbitrary constant. Using this two equations, u_0 is inversely proportional to the square root of the Prandtl number. Consequently, the Reynolds number scales as $\sqrt{\mathrm{Ra}}/\,\mathrm{Pr}$ and the Péclet number becomes proportional to the square root of the Rayleigh number as is clearly the case in Figure 10.

The Nusselt number defined by eq. (13) has been plotted in Figure 11 as a function of Ra and for the four Prandtl numbers already mentioned before. Clearly, the two regimes are identified: for Ra lesser than 10^3, the Nusselt number is constant while for Ra above 10^3 the Nusselt number increases with respect to Ra. Notice that the Nusselt in the conductive regime is larger than one due to the fact that without motion the temperature range is little smaller when the electrode length is shorter than the cavity height. For the Prandtl numbers equal to 10 to 10^3, profiles are completely similar meaning that the Prandtl number does not play a significant role. Moreover, a nonlinear fitting shows that the Nusselt number increases slowly with the Rayleigh number since the dependence is logarithmic as already pointed out by Sugilal et al. [21].

Both the Péclet and Nusselt numbers have been plotted in Figures 10 and 11 before a flow transition.
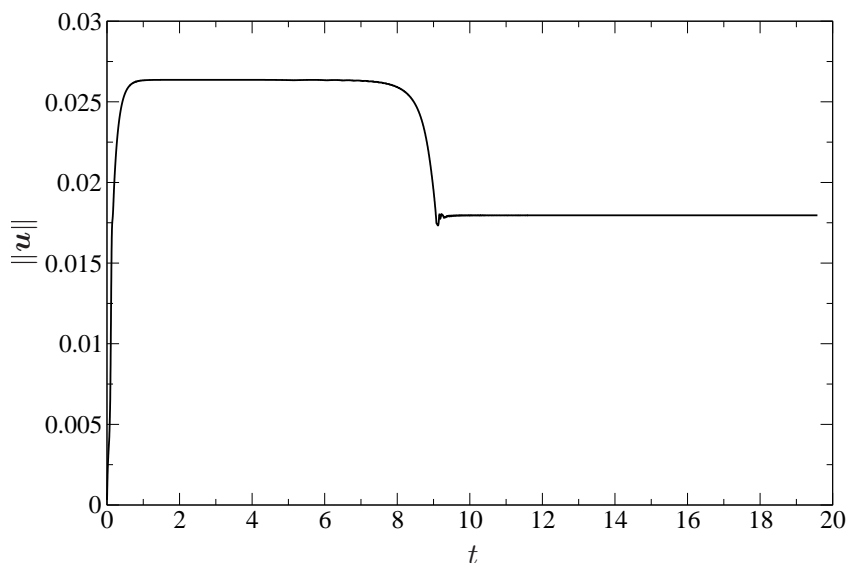
Figure 12: L^2-norm of $\boldsymbol{u}$ as a function of time obtained for $\mathrm{Pr} = 10^2$ and $\mathrm{Ra} = 3.5 \cdot 10^4$ for an enclosure with an aspect ratio equal to 2 and a length of electrodes equal $2/3$ of the cavity height.

Indeed, we observe numerically that over a Rayleigh number depending on the Prandtl number, the flow structure changes which can be seen in the behavior of the L^2-norm of the velocity given for example in Figure 12 when the Rayleigh number is equal to $\mathrm{Ra} = 3.5 \cdot 10^4$ and the Prandtl number is equal to $\mathrm{Pr} = 10^2$. After a fast increase, the velocity norm reaches a first plateau. When the time is larger than 7, the velocity decreases to reach a second plateau. The numerical solution is driven until the time convergence.

The modification of the flow structure can be seen by looking the iso-values of the temperature field as shown in Figure 13 for which six snapshots have been plotted. For the two first snapshots, the structures are symmetric obtained when the velocity reaches the first plateau in Figure 12. The observation of the stream function at the same times represented in Figure 14 allows to see the flow structure. For the two first snapshots, the flow structure is characterized by two counter-rotating cells. While at small times the temperature field is symmetric to the middle vertical axis, the symmetry is broken when the time becomes larger than 7 which is in the range where the L^2-norm of the velocity showing in Figure 12 decreases. The stream function shows that the left cell becomes more and more important instead of the right cell, see Figure 14. When the time is larger than 10, only one cell is observed leading to an asymmetric flow structure.

By using the time convergence of the numerical solution, the critical Rayleigh number over which the transition between the symmetric to asymmetric solutions has been determined. Indeed, when the symmetric solution is stable an exponential time convergence is observed. Conversely, when the transition appears, the time convergence of the symmetric is not present since an exponential increase is observed. Nevertheless, after the transition toward asymmetric solution, the time convergence is once again established [13]. Figure 15 presents the critical Rayleigh number $\mathrm{Ra_{cr}}$ as a function of the Prandtl number. A strong influence of the Prandtl number is observed when Pr is smaller than 10. For a Prandtl equal to one, the critical Rayleigh number is around $1.665 \cdot 10^5$ while above $\mathrm{Pr} = 10$, $\mathrm{Ra_{cr}}$ is approximately equal to $2.5 \cdot 10^4$ and does not change for larger Prandtl numbers.

By increasing the Rayleigh number, a second instability can be established. Indeed, numerical simulations have been done for a Rayleigh number larger or equal to $4 \cdot 10^4$ and for two Prandtl numbers
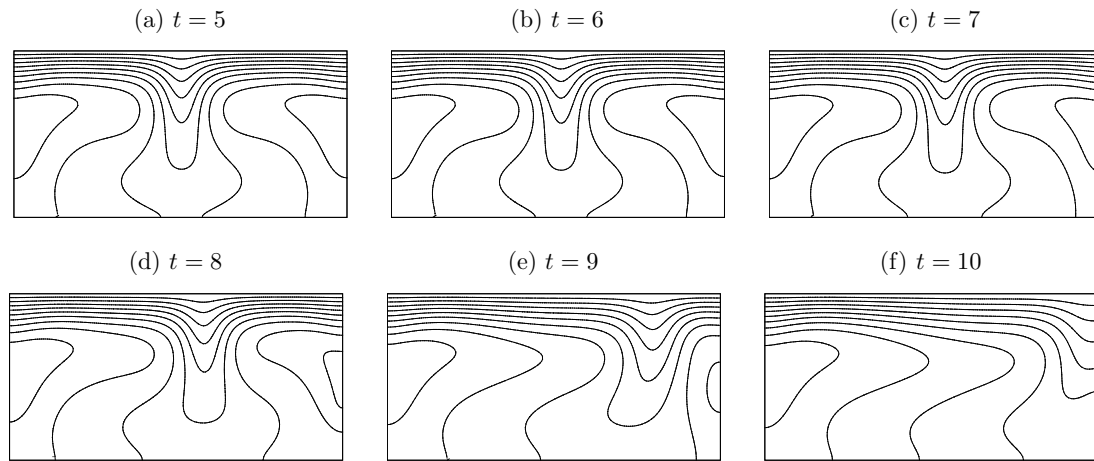
(a) $t = 5$ (b) $t = 6$ (c) $t = 7$

(d) $t = 8$ (e) $t = 9$ (f) $t = 10$

Figure 13: Snapshots of iso-values of the temperature field obtained for $\mathrm{Pr} = 10^2$ and $\mathrm{Ra} = 3.5 \cdot 10^4$ when time is equal to (a) $t = 5$, (b) $t = 6$, (c) $t = 7$, (d) $t = 8$, (d) $t = 9$ and (f) $t = 10$.
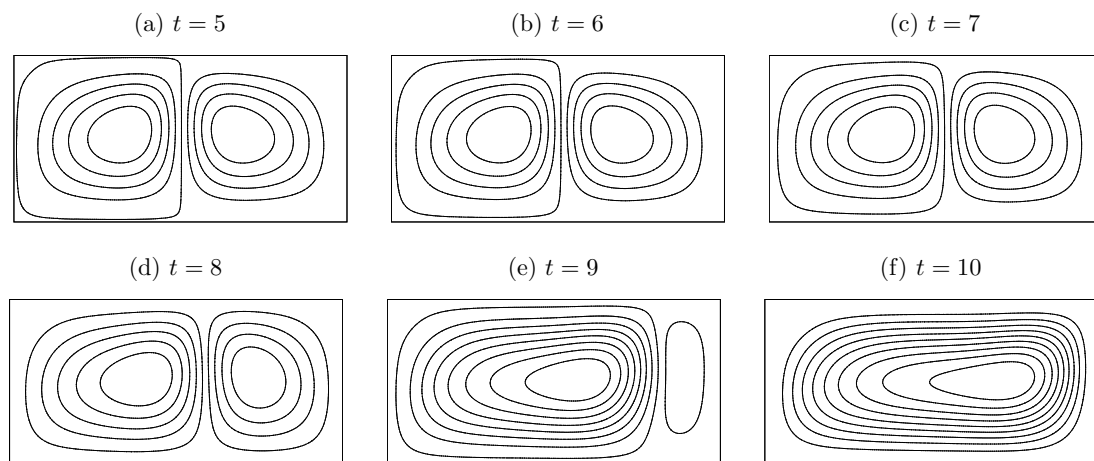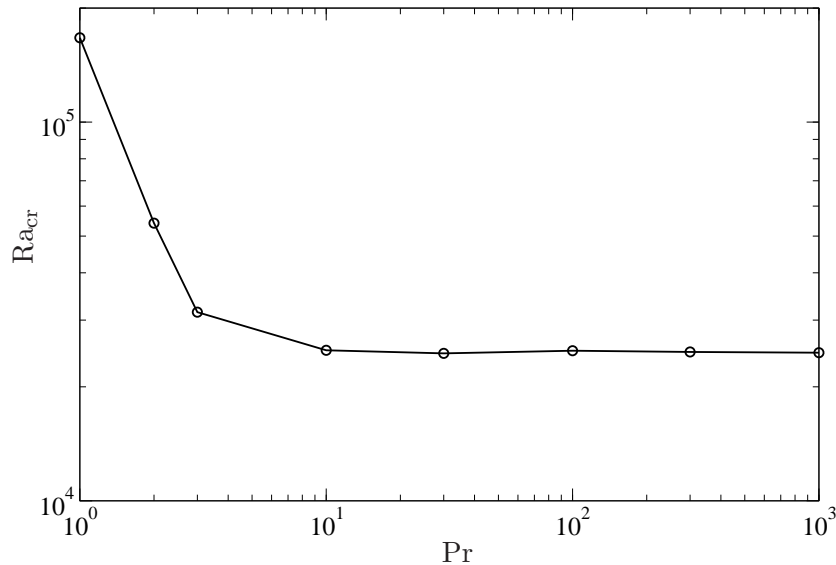
(a) $t = 5$ (b) $t = 6$ (c) $t = 7$

(d) $t = 8$ (e) $t = 9$ (f) $t = 10$

Figure 14: Snapshots of stream function obtained for $\mathrm{Pr} = 10^2$ and $\mathrm{Ra} = 3.5 \cdot 10^4$ when time is equal to (a) $t = 5$, (b) $t = 6$, (c) $t = 7$, (d) $t = 8$, (d) $t = 9$ and (f) $t = 10$.

Figure 15: Critical Rayleigh number $\mathrm{Ra_{cr}}$ above which the eigenvalue σ becomes positive as a function of the Prandtl number for a enclosure with an aspect ratio equal to 2 and a length of electrodes equal $2/3$ of the cavity height.

equal to 10 and 10^2. Figure 16 presents the behavior of the L^2-norm of the velocity for four Rayleigh numbers when the Prandtl number is equal to 10. As already seen in Figure 12, the norm of the velocity reaches rapidly a plateau corresponding to a symmetric flow structure followed by a decrease of the flow intensity.

Nevertheless, the flow becomes unsteady or more precisely periodic in time. Remark that the transition occurs earlier as the Rayleigh number increases. The periodic regime begins by an increase of the amplitude of oscillations and its duration gets shorter as Ra increases. Amplitudes of velocity oscillations grow with the Rayleigh number. Numerical simulations achieved for a Prandtl number equal to 10^2 and for four Rayleigh numbers present the same behaviors.

Since it is difficult to analyze the periodic regime from the previous figures, we perform a Fourier analysis for the eight simulations. Only the range in time for which the flow is fully periodic has been used to determine the Fourier spectra. Figure 17 depicts the Fourier spectra obtained for the two Prandtl numbers and various Rayleigh numbers. Signals are very close to a sinusoidal behavior with a fundamental frequency with an amplitude corresponding to the velocity oscillation seen in Figures 16. Second pics are observed at a frequency equal to a second harmonic of the signal but with an amplitude much smaller.

Figure 18 presents the behaviors of the fundamental frequencies versus Rayleigh number for the two Prandtl numbers on the left of the figure. For the two cases, the frequency grows linearly with the Rayleigh number. In Figure 18-(b) the amplitude of the Fourier spectra multiplied by $\sqrt{\mathrm{Ra}\,\mathrm{Pr}}$ has been plotted as a function of Ra. By this way, amplitudes obtained for the two Prandtl numbers scales very well. In fact this result is expected since by multiplying by $\sqrt{\mathrm{Ra}\,\mathrm{Pr}}$ the normalized of the velocity scales as a Péclet number. So, previously, we showed that the Péclet number scales very well with the Rayleigh number.

According to the results obtained for the two Prandtl numbers and Rayleigh numbers larger than the critical value, the onset of unsteady flow seems similar to a Hopf bifurcation. After a transition regime, the oscillating solution appears with a growth depending on the Rayleigh number. Close to the transition,
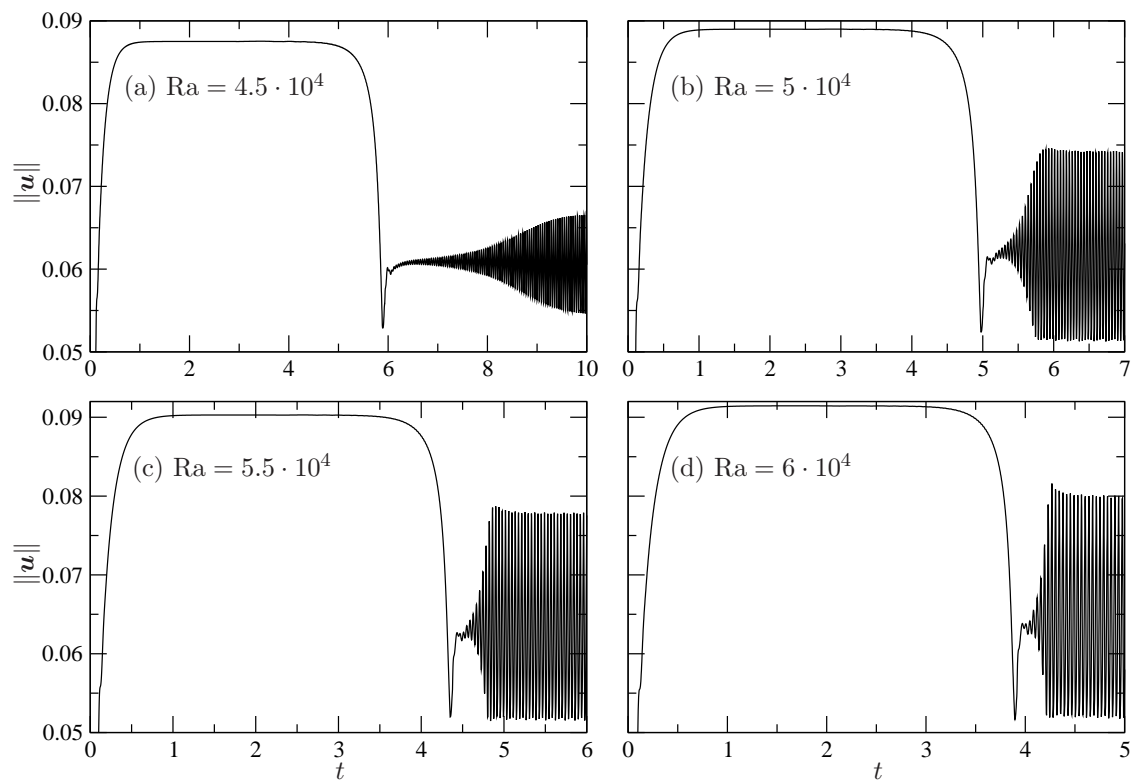
Figure 16: $\|\boldsymbol{u}\|$ as a function of t for $\mathrm{Pr} = 10$ and (a) $\mathrm{Ra} = 4.5 \cdot 10^4$, (b) $\mathrm{Ra} = 5 \cdot 10^4$, (c) $\mathrm{Ra} = 5.5 \cdot 10^4$ and (d) $\mathrm{Ra} = 6 \cdot 10^4$.
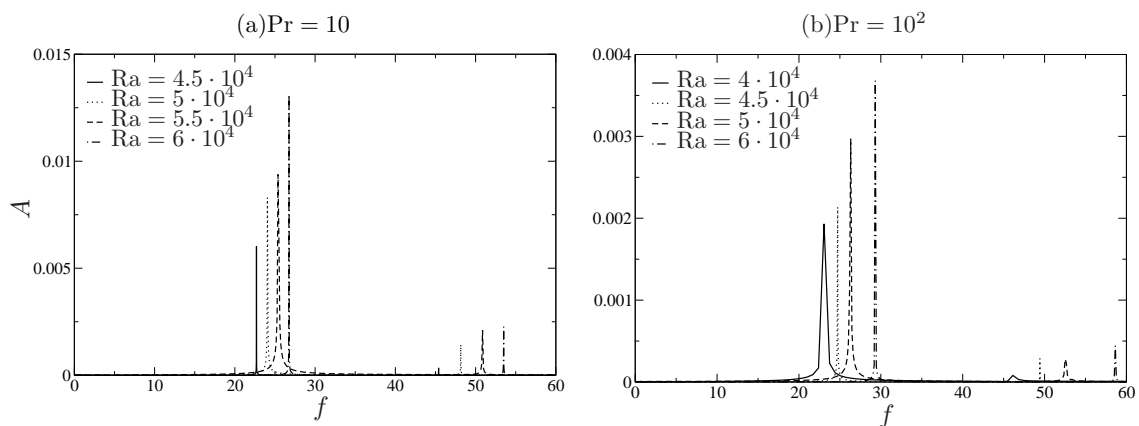
Figure 17: Fourier spectra of the norm of $\|\boldsymbol{u}\|$ for $\mathrm{Pr} = 10$ and for $\mathrm{Pr} = 10^2$ and Rayleigh numbers larger than $4 \cdot 10^4$.
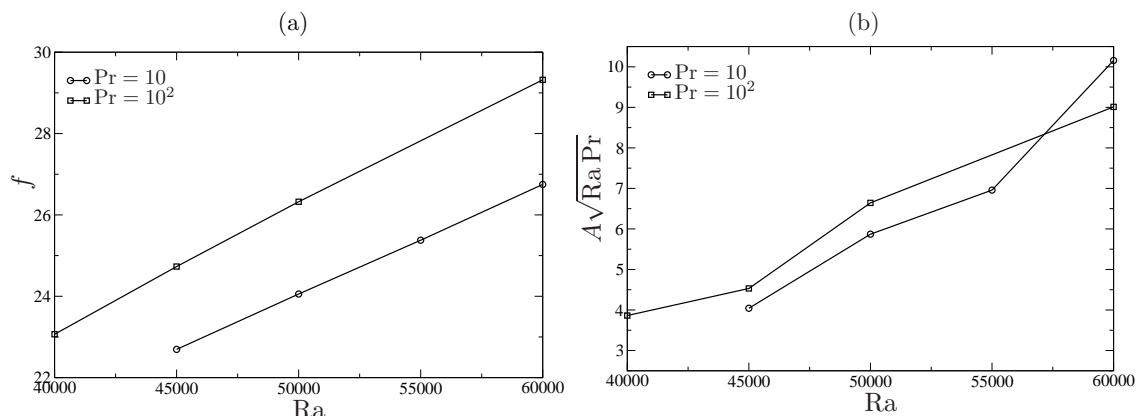
Figure 18: Behaviors of the Fourier spectra for the Prandtl numbers equal to 10 and 10^2, (a) f vs. Ra and (b) $A\sqrt{\text{Ra}\,\text{Pr}}$ vs. Ra.

the establishment of the limit cycle takes more time. Another fact justifying the nature of the bifurcation is that the frequency of the velocity fluctuations is linear with the control parameter, i.e. the Rayleigh number.

5   Conclusion

This work has been devoted to the thermo-convection in a Joule-heated cavity. A non-uniform volumetric heat source is produced by an electric field applied with two vertical electrodes localized on the vertical walls of the enclosure. The coupled of Navier-Stokes heat transfer and electric potential equations are solved using a discontinuous Galerkin finite element technique. The solver is tested in a situation for which the heat source is uniform in volume leading to a threshold in convection like in a classical Rayleigh-Bénard convection. The critical Rayleigh number is determined.

After this preliminary test validating the numerical solver, we shorten the electrodes with a length equal at $2/3$ of the cavity height. In such a case, the threshold disappears and the flow starts to exist as soon as the Rayleigh number is larger than zero. Numerical simulations have been done for a large range of Prandtl number, between 1 to 10^3. The convection intensity can be characterized in term of Péclet number. Two regimes arise: one obtained when the Rayleigh number is smaller than 10^3 exhibiting a linear behavior of the Péclet number versus the Rayleigh number; the second regime is characterized by a square root dependency of the Péclet number as a function of Rayleigh number.

By increasing the Rayleigh number, the flow does not stay stable. Below the transition, the flow structure is symmetric over the vertical middle axis. Above the transition, the flow structure becomes asymmetric for which the two symmetric cells are replaced by one cell. Using the behavior of the convergence toward the steady-state regime, we establish the behavior of the critical Rayleigh number as a function of the Prandtl number. At small Prandtl number, the dependency on the critical Rayleigh number is very important. However, when the Prandtl number is larger than 10, the critical Rayleigh number does not change significantly and is equal to $2.5 \cdot 10^4$.

By analyzing the flow obtained for Rayleigh numbers larger than the critical values, we pinpoint that the onset of periodic solution obeys to a Hopf bifurcation.

In term of industrial process, the occurrence of an unsteady flow leads to a difficult control of the industrial plant. In glass industry, the typical Rayleigh number is always larger than the critical value found

in the present study. Moreover, we observe that the flow structure can change dramatically which can be harmful for working conditions.

Acknowledgements

References

[1] M. Abramowitz and I. A. Stegun. *Handbook of mathematical functions*. Dover Publications, Inc., New York, 1965.

[2] A. Bejan. *Convection heat transfer*. John Wiley & Sons, New York, 1995.

[3] M. K. Choudhary. A three-dimensional mathematical model for flow and heat transfer in electrical glass furnaces. *IEEE Trans. Ind. Appl.*, IA-22(5):912–921, 1986.

[4] B. Cockburn, G. Kanschat, D. Schötzau, and C. Schwab. Local discontinuous galerkin methods for the Stokes system. *SIAM J. Numer. Anal.*, 40(1):319–342, 2002.

[5] D. A. Di Pietro and A. Ern. *Mathematical aspects of discontinuous Galerkin methods*. Springer-Verlag, Heidelberg, 2012.

[6] A. Ern and J.-L. Guermond. *Eléments finis : Théorie, applications, mise en œuvre*. Springer, Paris, 2002.

[7] J.-M. Flesselles and F. Pigeonneau. Kinematic regimes of convection at hight Prandtl number in a shallow cavity. *C. R. Mécanique*, 332:783–788, 2004.

[8] S. Gopalakrishnan, A. Thess, G. Weidmann, and U. Lange. Chaotic mixing in a Joule-heated glass melt. *Phys. Fluids*, 22(1):013101, 2010.

[9] D. D. Joseph. *Stability of fluid motions II*. Springer-Verlag, Berlin, 1976.

[10] Ruby Krishnamurti. Some further studies on the transition to turbulent convection. *J. Fluid Mech.*, 60(02):285–303, 1973.

[11] F. A. Kulacki and R. J. Goldstein. Hydrodynamic instability in fluid layers with uniform volumetric energy sources. *Appl. Sci. Res.*, 31(2):81–109, 1975.

[12] P. Manneville. *Instabilities, Chaos and Turbulence*. World Scientific Publishing Company, 2004.

[13] F. Pigeonneau, A. Cornet, and F. Lopépé. Thermoconvective instabilities of a non uniform Joule-heated liquid enclosed in a rectangular cavity. *J. Fluid Mech.*, 2017. under consideration.

[14] F. Pigeonneau and J.-M. Flesselles. Practical laws for natural convection of viscous fluids heated from above in a shallow cavity. *Int. J. Heat Mass Transfer*, 55:436–442, 2012.

[15] P. H. Roberts. Convection in horizontal layers with internal heat generation. theory. *J. Fluid Mech.*, 30(01):33–49, 1967.

[16] C. P. Ross and G. L. Tincher. *Glass Melting Technology: A Technical and Economic Assessment*. Glass Manufacturing Industry Council, Werterville (OH, USA), 2004.

[17] P. Saramito. *Efficient C++ finite element computing with Rheolef*. CNRS-CCSD ed., 2015.

[18] P. Saramito. *Efficient C++ finite element computing with Rheolef: vol. 2. Discontinuous Galerkin methods*. CNRS-CCSD ed., 2015.

[19] H. Scholze. *Glass. Nature, Structures and Properties*. Springer-Verlag, Berlin, 1990.

[20] J. Stanek. *Electric melting of glass*. Elsevier, Paris, 1977.

[21] G. Sugilal, P. K. Wattal, and K. Iyer. Convective behaviour of a uniformly Joule-heated liquid pool in a rectangular cavity. *Int. J. Therm. Sci.*, 44:915–925, 2005.

[22] E. Süli and D. F. Mayers. *An Introduction to Numerical Analysis*. Cambridge University Press, Cambridge (UK), 2003.

[23] R. Thirlby. Convection in an internally heated layer. *J. Fluid Mech.*, 44(04):673–693, 1970.

[24] K. E. Uguz, G. Labrosse, R. Narayanan, and F. Pigeonneau. From steady to unsteady 2-D horizontal convection at high Prandtl number. *Int. J. Heat Mass Transfer*, 71:469–474, 2014.

[25] R. Viskanta and E. E. Anderson. Heat transfer in semitransparent solids. *Advances in heat transfer*, 11:317–441, 1975.